Chapter 11

Spinel-Structured Nanoparticles for Magnetic and Mechanical Applications

Malik Anjelh Baqiya, Ahmad Taufiq, Sunaryono, Khuroti Ayun, Mochamad Zainuri, Suminar Pratapa, Triwikantoro and Darminto

Additional information is available at the end of the chapter

http://dx.doi.org/10.5772/66293

Abstract

Nanoparticles of Fe_3O_4 have been successfully synthesized using a simple coprecipitation technique from natural iron sands, employing HNO_3 and NH_4OH as dispersing and precipitating agents, respectively. The substitution of Fe with Mn to result in $Fe_{3-x}Mn_xO_4$ ($0 \le x \le 3$) was conducted to control the magnetic strength of this nano-sized spinel powder. It is shown that magnetic properties depend not only on the particle size and Mn doping but also on the particles clustering. The applications for magnetic fluids, gels, and coating are extensively described. Meanwhile, the spinel $MgAl_2O_4$ nanoparticles have also been prepared by the same simple method from commercial starting materials. This powder was used as a nano-reinforcer of Al-matrix composites. In addition, $MgAl_2O_4$ micro-sized powder forming a thick layer was successfully grown by electroless plating on the interface of matrix-filler in Al/SiC composites. The strengthening of mechanical properties with respect to the varying uses of these $MgAl_2O_4$ powders is discussed.

Keywords: Fe_3O_4, $MgAl_2O_4$, Powders, Coprecipitation, Magnetic, mechanical properties

1. Introduction

Spinel structures have the general formula of AB_2X_4, where X can be oxygen (oxides) or a chalcogen element, such as sulfur (thio-spinels) and selenium (seleno-spinels). A and B in the spinel structures can be divalent, trivalent, or tetravalent cations, such as iron, magnesium,

aluminum (Al), zinc, manganese, chromium, and titanium. The various compounds of spinel family including their chemical and physical properties depend not only on the arrangement of cations and anions in the structures but also on how the spinels are produced. The spinels can be magnetic or non-magnetic compounds depending on the nature of the cations among the A and B sub-lattices. Fe_3O_4 ($FeO.Fe_2O_3$) is one of the so-called spinel ferrite having magnetic properties, whereas $MgAl_2O_4$ is also spinel (should not be confused with the spinel structure described earlier) which is non-magnetic one. This chapter covers some of the physical properties of the spinel compounds in more detail.

2. Magnetite (Fe_3O_4) nanoparticles

Fe_3O_4 (magnetite) or the black iron oxide in the form of nanoparticles has huge potential for applications in many fields. However, preparing Fe_3O_4 particles in small size with high quality is enormously challenging for several reasons. Therefore, the preparation of Fe_3O_4 nanoparticles in several forms and various sizes with high purity and homogeneity becomes an essential task before applications. The following section provides more details on the preparation and applications of Fe_3O_4 nanoparticles.

Several synthesis methods to prepare high-purity Fe_3O_4 nanoparticles in various forms and sizes have been reported in the literature. In general, Fe_3O_4 nanoparticles have been successfully prepared through sonochemical [1], thermal decomposition [2], ionothermal [3], hydrothermal [4], micro-emulsion [5], sol-gel [6], modified hydrolysis [7], solvothermal [8], electrospinning [9], coprecipitation [10] methods, and so forth. However, high quality of the particles, such as good particle size distribution with high crystalline, structural and compositional homogeneity, still has become one of the main challenges in preparing Fe_3O_4 nanoparticles [11].

The improvement of synthesis methods has also been carried out for producing Fe_3O_4 nanoparticles in order to reduce cost and time of preparation. A simple method to produce Fe_3O_4 nanoparticles via coprecipitation method has been introduced using a local natural iron sand from Indonesia as a starting material. This coprecipitation method is considered to be the easiest method for preparing Fe_3O_4 nanoparticles [12] because of its simplicity, efficiency, and inexpensiveness [13]. The use of starting material from commercial product can be substituted by natural iron sand.

As for the preparation of Fe_3O_4 nanoparticles using coprecipitation method, the ratio of ferrous and ferric ions is very crucial affecting the synthesis result. The effects include the particle diameter and magnetic properties. Iida et al. [14] have reported that the valence of the metal salt is an important factor for determining the particle size of the magnetic particles. In their experiments, they have succeeded in obtaining Fe_3O_4 nanoparticles in the size range of 9–40 nm with various molar contents of ferrous ions in the total amount of the iron ions. Furthermore, Gnanaprakash et al. [15] have also reported that initial pH and temperature of the iron salt solution during coprecipitation process have strong influences for the formation of magnetite nanoparticles. They reported that the average of particle size having initial pH value

of 0.7, 1.5, 3, and 4.7 are 6.7, 7.6, 9.9, and 9.9 nm, respectively. Determination of particle size is very important according to how they will be used for certain applications, namely for magnetic fluids and gels.

In the magnetic nanoparticles' syntheses, the so-called templating method has been employed to form certain particle shapes and sizes, such as one dimensional (1-D) particles or nanorods. Lian et al. [16] have successfully synthesized nanorods of Fe_3O_4 through the addition of polyethylene glycol (PEG) 1000 as a template with the average particle diameter and length of 80 nm and 2 μm, respectively. Therefore, templating technique has important role on the particle growth of magnetic nanomaterials. The greater value of the PEG's molecular weight will lead to the higher possibility to obtain nanorods resulted from the synthesis [17]. Furthermore, based on the research of He et al. [18], Fe_3O_4 nanowire has successfully been prepared depending on the volume ratio of PEG and H_2O. They have found that the best formation is achieved with the ratio of 1:3; a higher ratio gives higher viscosity and inhibits the particle formation.

3. Fe_3O_4 spinels for magnetic fluids and gels

Generally, the study of Fe_3O_4 nanoparticles has attracted attention for several disciplines. Physicists investigate the physical properties and propose the theories of the Fe_3O_4 nanoparticles. Chemists focus on the synthesis methods of the Fe_3O_4 nanoparticles. Biologists concentrate on developing Fe_3O_4 nanoparticles in bioapplications. Meanwhile, engineers study Fe_3O_4 nanoparticles with a focus on technological applications. Therefore, there is a great deal of interest in Fe_3O_4 nanoparticles by scientists and engineers, starting from synthesis and characterizations and followed by their many application potentials.

Fe_3O_4 ferrofluids or magnetic fluids are colloidal suspension containing magnetite nanoparticles in single domain, which are dispersed in a liquid carrier. Ferrofluids have unique characteristics because they have both the liquid and magnetic properties. In the ferrofluids, the liquid carriers can be polar or nonpolar medium. In order to prevent agglomerations, the Fe_3O_4 nanoparticles should be layered or covered by an appropriate material as a shell [19]. In the last decades, it has been reported that the Fe_3O_4 ferrofluids can be applied in various fields, that is, optical grating, optical switching [20], thermoelectric conversion [21], quenching media [22], sensor [23], controlling lubricant migration [24], biomedical applications [25], and so forth.

Another application for the magnetite spinel is in ferrogels, namely a hydrogel containing magnetic ferrous particles. The Fe_3O_4-ferrogel can be defined as a polymer (nano)composites with polyvinyl alcohol (PVA) and Fe_3O_4 as the matrix and filler, respectively, cross-linked together with a certain amount of liquid (water). Ferrogels can be physically or chemically cross-linked without any chemical reaction between them. The physical properties of ferrogels depend on the preparation conditions, such as polymer and solvent ratio, particle size, distribution and concentration of the magnetic material. By combining the elastic medium and the magnetic properties from the particles, the elastic behavior of ferrogel can be manipulated

by external magnetic field. This leads to a great opportunity for various advanced applications, namely soft actuators and artificial muscles [26].

In the development of magneto-elastic materials, Li et al. [27] have prepared a polymeric gel in variety of shapes depending on the temperature. Furthermore, Zrínyi et al. [28] have developed a magneto-sensitive gel with Fe_3O_4 as the magnetic filler. Ramanujan and Lao [26] have successfully produced magnetic gel consisting of PVA and micro-sized Fe_3O_4 particles for artificial tissues. They have demonstrated an elastic behavior of the gel controlled by an external magnetic field.

4. Spinel $MgAl_2O_4$ grown as a thick coating and fillerreinforcer in composites

Compared to the conventional aluminum alloys, aluminum metal matrix composites (Al-MMC) have been used in many kinds of applications (e.g. automobiles) due to their high specific strength and Young's modulus, improved yield and creep strengths, light weight, and excellent properties of wear resistance. The important parameter for improving their performances lies in the structure and bonding properties between the matrix and fillers. Some materials in any form of particles have been widely used as the particle-matrix interfaces in order to improve the wettability [29], namely MgO, SiC, and Al_2O_3 in the micro- or nanostructures. It has been noted that the interface, particles size, and its distribution as well as the concentration (volume fraction) play a basic role in the modification of Al-MMC.

A typical way to improve the mechanical properties of Al-MMC is by additional reinforcement or interfacial modification. Recently, the spinel $MgAl_2O_4$ has been applied for this purpose. In the last decade, $MgAl_2O_4$ has been produced by several methods such as solid-state reaction [30], high-energy ball milling [31], polymerization method [32], pyrolysis [33], sol-gel processes [34, 35], and coprecipitation techniques [36–38]. The shape and size of the spinel particles vary depending on the preparation techniques [39, 40]. This spinel can be prepared in the form of ceramic foams [41, 42], whiskers [43–45], thin films [46, 47], nanoparticles [37, 48, 49], and also layer of particle bonding in composite materials [50]. For the Al/SiC composites, in which Al acts as the matrix and SiC acts as the filler reinforcement, Al_4C_3 phase can be formed at the interface between matrix and fillers. This phase weakens the mechanical strength of the composite. Up to now, several experimental techniques have been proposed to prevent this problem including adding excessive Si into the matrix and introducing a thin coating layer on the SiC particle surface. The formation of interlayer phase is believed to be a stable interfacial bonding that improves the mechanical properties of the composite. However, the detail of this mechanism remains unclear.

Particulate-reinforced composites with micron-sized filler of various materials are the most commonly used composites in daily life. Particles are typically introduced to enhance the matrix elastic modulus and yield strength. It has been shown that the novel properties of composites are improved by adding nano-scaled particles as the fillers [51]. The key role of mechanical strength in composites is the interface-bonding quality between matrix and filler

http://dx.doi.org/10.5772/66293

materials. The nano-sized particles have much greater total area compared to particles with larger size at the same volume. The interface interaction can therefore be extended by reducing particle size of fillers down to nanometer scale.

Meanwhile, synthesis of particles in nanometer size of various materials is still an active area of research. Because of their very small size, nanoparticles tend to be aggregate to each other to form larger size particles [52]. As nanometer-scaled filler, the particles have to be kept separate in the matrix. In this context, an effort to maintain nanoparticles as fillers from agglomeration was achieved by the introduction of a surfactant. Tetra-methyl-ammonium-hydroxide (TMAH) could be used as surfactant in the process of filler-matrix-mixing media. Aluminum was chosen as matrix, while MgO and $MgAl_2O_4$ were used as nano-fillers. In the case of Al/SiC composites, a thin-layer $MgAl_2O_4$ is coated onto the SiC filler to enhance matrix-filler interfacial bonding leading to increased mechanical strength. The SiC fillers were coated by spinel $MgAl_2O_4$ by electroless plating, soaking SiC particulate powder in solutions containing Mg and Al ions before heating process to grow spinel phase on the surface.

5. Preparation of Fe_3O_4 nanoparticles from iron sands

The detail of synthesis method for the preparation of Fe_3O_4 nanoparticles was described in our previous works [53–57]. The iron sand was extracted by a magnetic separator to obtain dominantly Fe_3O_4 powders. Using a magnetic stirrer, the hydrochloric acid (HCl) was used to dissolve the Fe_3O_4 powder to produce $FeCl_3$ and $FeCl_2$ solutions at room temperature as written in Eq. (1).

$$Fe_3O_4 + 8HCl \rightarrow 2FeCl_3 + FeCl_2 + 4H_2O \quad (1)$$

The solution of $FeCl_3$ and $FeCl_2$ was then reacted by dropping slowly ammonium hydroxide (NH_4OH) to produce black precipitate at room temperature. The reaction mechanism for producing Fe_3O_4 particles is described as Eq. (2) [54]

$$2FeCl_3 + FeCl_2 + 8NH_4OH \rightarrow Fe_3O_4 + 8NH_4Cl + 4H_2O \quad (2)$$

In order to synthesize $Mn_xFe_{3-x}O_4$ nanoparticles discussed later and investigate its magnetic properties, the variation of Mn concentration from $MnCl_2$ solution was also prepared to form $Mn_xFe_{3-x}O_4$ ($0 < x \leq 1$). The dissolved $MnCl_2$ solution was mixed using a magnetic stirrer followed by a drop-wise addition of NH_4OH to obtain the precipitate of Fe_3O_4 and $Mn_xFe_{3-x}O_4$. The magnetic moment of Mn^{2+} ion is 25% higher than that of Fe^{2+} ion. Therefore, introducing Mn^{2+} into Fe_3O_4 to form $Mn_xFe_{3-x}O_4$ structure will theoretically enhance the magnetization of Fe_3O_4 [58]. A washing process of the precipitate was then carried out for several times using distilled water until achieving normal pH condition. Finally, the Fe_3O_4 powders were prepared by drying process at 100°C for 1 h. For the preparation of Fe_3O_4 magnetic fluid, tetra-methyl-

ammonium-hydroxide (TMAH), as the stabilizing layers of the particles, was added in the precipitate. In the present investigation, Fe_3O_4 ferrogels were also synthesized using freezing-thawing method as described in Refs. [57, 59].

To study the crystal structure, the particle size and its distribution as well as form and structural factor, and the magnetic properties of the sample, the Fe_3O_4 powders were then characterized by means of X-ray diffractometry (XRD), small-angle neutron scattering (SANS) spectrometer and superconducting quantum interference device (SQUID) magnetometer, respectively. The XRD measurements were carried out in the 2θ range from 20° to 70° using Cu-Kα radiation. A 36-m SANS spectrometer was used to investigate the primary and secondary particles as well as the fractal structure of Fe_3O_4 nanoparticles. The detailed SANS measurements have been given elsewhere [54, 60]. The two-lognormal analysis was also performed to investigate the clustering effect of the magnetic fluid and hydrogel [55, 57].

6. Preparation of spinel $MgAl_2O_4$ as filler reinforcers

Magnesium oxide (MgO) and magnesium-aluminum oxide ($MgAl_2O_4$) as fillers were synthesized by employing coprecipitation process. Mg (Aldrich, 99.9%) and Al (Aldrich, 99.9%) were dissolved in HCl (12.63 molar) with stoichiometric molar fraction. The NH_4OH (6.5 molar) was used as precipitating agent to produce $Mg(OH)_2$ and $MgAl_2O_4$ after filtering, washing process with distilled water for several times, and finally drying at 100°C. The resulting powders were then heated at 500°C for 1 h to convert them into MgO and $MgAl_2O_4$ phases. The powders were checked with XRD and transmission electron microscope (TEM) to explore the phase purity, crystallite size, particle shape, and size.

The MgO and $MgAl_2O_4$ powders were mixed with TMAH as surfactant to form a colloid system, consisting of individual MgO or $MgAl_2O_4$ particles which were homogeneously dispersed. To fabricate composites, Al powders as matrix were added into the colloid system and followed by thorough stirring and grinding to achieve homogeneity. The mixed powders were dried at 100°C for 3 h and then pressed into pellets having a diameter of 1 cm. During pelletization, the powders were compacted using a force of 1.5 kN applied for 15 min in an isostatic die with zinc stearate on the inner disc. Before sintering process at 500°C for 1 h, pellets were pre-sintered at, respectively, 200 and 400°C for 20 min each. All heat treatments were conducted in a furnace with a controlled atmosphere of low vacuum ($\sim 10^{-3}$ atm).

The samples produced consist of Al/MgO and Al/$MgAl_2O_4$ composites with various volume fractions (% vol) of fillers covering 10, 20, and 30%. We have also prepared the corresponding samples fabricated without TMAH for comparison. To study the effects of surfactant addition during the process on the fabricated composites, measurements of densities, porosity, elastic modulus by compressive test, and microhardness (Vicker's hardness number, VHN) of the samples were carried out.

Furthermore, to prepare the Al/SiC composites, the aluminum (PA) powders and particles of SiC ceramics (220 mesh) were employed as starting materials. The SiC reinforcement particles

http://dx.doi.org/10.5772/66293

were cleaned by ultrasonic cleaner in alcohol (90%), and then dried in oven at 100°C. The SiC particles were then soaked in an electrolyte media of 40 ml HNO_3 containing Al and Mg ions as the part of the electroless-plating mechanism. The process of metal oxide coating was done using a magnetic stirrer at 125°C. The oxidation of SiC particles to grow the $MgAl_2O_4$ layer was performed in a furnace at 200°C for 1 h, and continued at 400°C for another 1 h. The electrolyte media for electroless plating can be controllably adjusted to grow various metal oxides on the SiC surface, such as MgO, CuO, Al_2O_3, and so forth, besides $MgAl_2O_4$. The metal oxide-coated SiC particles were mixed with Al powders in n-butanol (wet mixing) using magnetic stirrer at 100°C, having SiC volume fraction (%vol) of 10, 20, and 30%. The heating process of the green pellets was carried out in a vacuum (10^{-3} Torr, rotary pump) by applying a pre-sintering at 200°C for 20 min and followed by sintering at 600°C for 1 h.

7. Results and discussion

7.1. Fe_3O_4 nanoparticles: magnetic properties and applications

The XRD pattern of Fe_3O_4 nano-powders is shown in **Figure 1**. All peaks in the pattern show a single phase of spinel structure corresponding to the crystal structure of Fe_3O_4 with PDF No. 19-0629 without any impurity. Based on the Rietveld analysis, the sample has lattice parameter $a = b = c$ of approximately 8.377 Å.

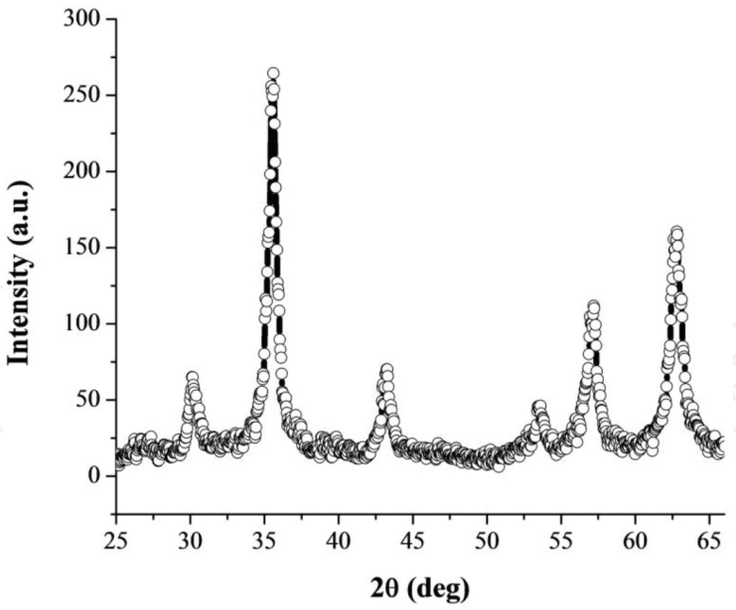

Figure 1. The XRD pattern of Fe_3O_4 nano-powders (using Cu-Kα radiation).

The SANS pattern of the Fe_3O_4 nano-powders is presented in **Figure 2**. The SANS data were analyzed using a lognormal spherical model as a form factor $P(R)$ and mass fractal model as a structure factor $S(q)$, following Eqs. (3) and (4), respectively,

$$P(R) = \frac{1}{\sigma R\sqrt{2\pi}} \exp\left(\frac{\ln^2(R/R_0)}{2\sigma^2}\right) \tag{3}$$

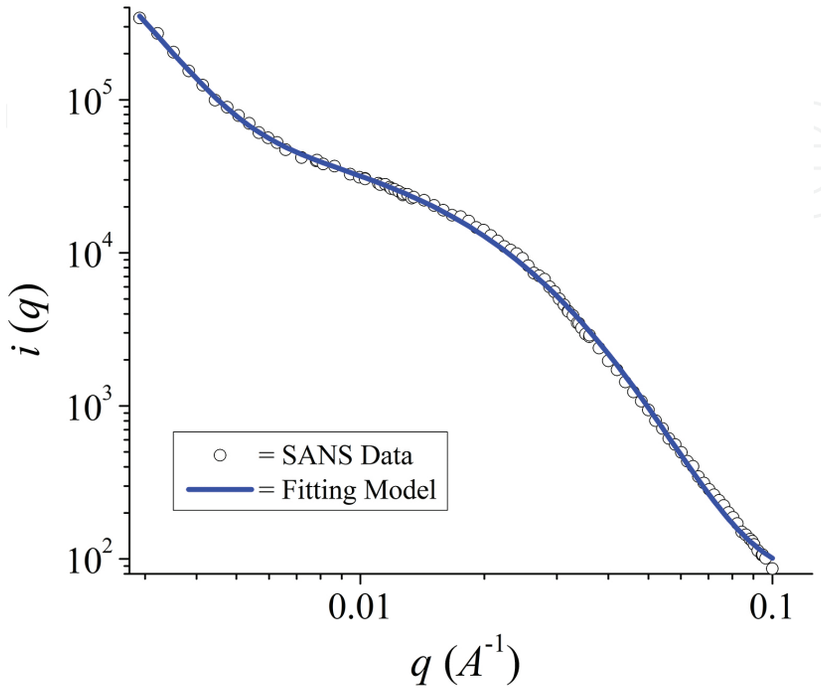

Figure 2. SANS data of Fe_3O_4 nano-powders.

with R_0 and σ representing the radius of the distribution and standard deviation, respectively [61],

$$S(q) = 1 + \frac{D\Gamma(D-1)}{(qR)^D\left[1+1/(q^2\xi)^2\right]^{(D-1)/2}} \sin\left[(D-1)\tan^{-1}(q\xi)\right] \tag{4}$$

where q, Γ, D, and ξ represent the scattering vector, gamma function, fractal dimension, and cut-off distance, respectively [62]. The SANS curve was fitted globally using two lognormal spherical model as form factor combining with mass fractal model as structure factor regarding Eq. (5) [54]

$$I(q) \approx \int_0^\infty N_1(R_1) F_N^2(q,R_1) dR_1 + \int_0^\infty N_2(R_2) F_N^2(q,R_2) dR_2 S(q,\xi,D,R_2) \tag{5}$$

Here, I is the density, N is the number density of particles, R_1 is the primary particles, R_2 is the secondary particles or clusters, and F is the scattering amplitude.

http://dx.doi.org/10.5772/66293

Based on the analysis using lognormal and mass fractal models, the Fe_3O_4 nano-powders have hierarchical nanostructure with the primary particles of 3.8 nm as a building block constructing secondary particles as clusters of 9.3 nm. The clusters of Fe_3O_4 nanoparticles have a fractal structure in three-dimension with fractal dimension of 2.9. The SANS data analysis of magnetic nanoparticles coincides with the image produced by high-resolution transmission electron microscopy (HRTEM) as shown in the previous work [54]. The details of the analysis of SANS data of the Fe_3O_4 nanoparticles were presented in the previous work [54].

The magnetic properties of the Fe_3O_4 nanoparticles as well as M versus H variations and zero-field-cooling (ZFC) curves are presented in **Figures 3** and **4**. The M versus H curve of the Fe_3O_4 nanoparticles was collected at room temperature by sweeping the magnetic field from -5 to 5 T. The Fe_3O_4 nanoparticles have saturated magnetization of 37.1 emu/g. Regarding **Figure 3**, it is clear that the M-H curve of sample has S-shape with nearly zero coercivity field, indicating the superparamagnetic behavior at room temperature. This result is consistent with the recent paper by Abboud et al. [63] where the magnetization was almost zero in the absence of external magnetic field. The superparamagnetic phenomenon in the magnetic nanoparticles has also been observed in the Fe_3O_4@SiO_2 core-shell composites [64], the dispersed Fe_3O_4 in the polymer matrix [65], and Fe_3O_4-$LiMo_3Se_3$ [66]. Moreover, the zero-field-cooling (ZFC) measurement was also carried out to investigate the superparamagnetic phenomenon of the sample as shown in **Figure 4**. Based on the results in **Figure 4**, it is evident that the sample has a maximum peak of magnetic blocking temperature, T_B, at 243 K. Theoretically, T_B depends on the particle size and shape so the increase of nanoparticle's volume will increase the T_B value [67].

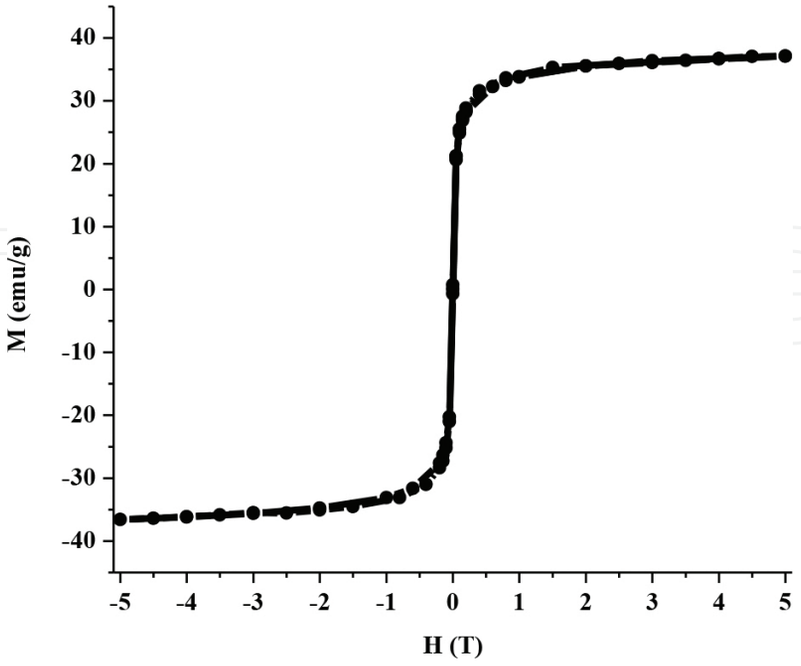

Figure 3. M-H curve of Fe_3O_4 nanoparticles at room temperature.

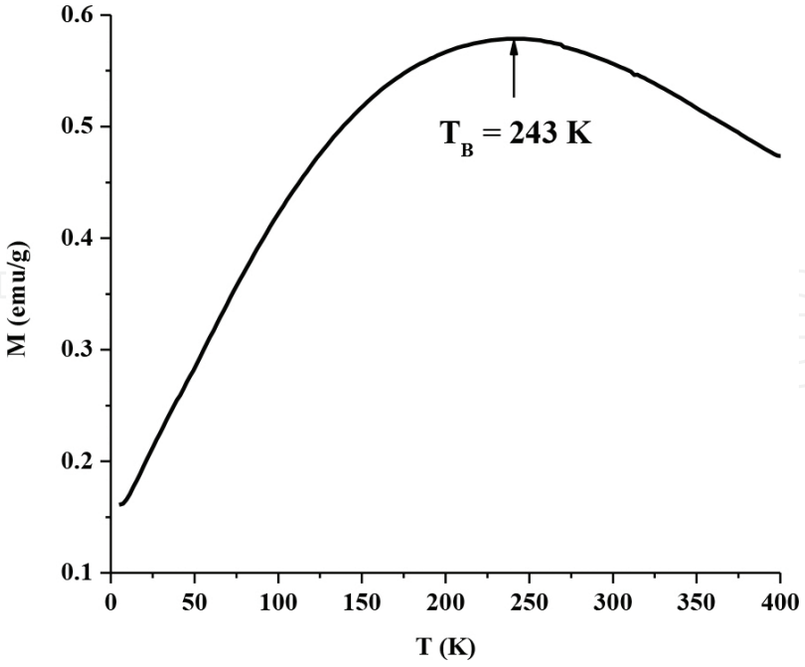

Figure 4. Zero-field-cooling (ZFC) curve of Fe_3O_4 nanoparticles (T_B = 243 K).

Dutta et al. [68] have reported that Fe_3O_4 nanoparticles with the particles size ranging from 4 to 12 nm have blocking temperature lower than 100 K, which is not similar to the result of this work. The difference of these results can be explained in a sense of the presence of clusters or aggregations phenomena in the present work. In Ref. [68], the samples were constructed with primary particles in relatively homogeneous samples without any clusters or aggregations. On the other hand, the sample in this work consists of hierarchical nanostructures of primary particles forming secondary particles or clusters with fractal dimension in three-dimensions. Despite the particles size and anisotropy constant, the clusters of magnetic nanoparticles give an effect on the blocking temperature. Theoretically, at magnetic-blocking temperature, the thermal energy of particles is comparable with the anisotropy energy barrier. In bulk, the Fe_3O_4 is ferrimagnetic generated by net magnetic moments at tetrahedral and octahedral sites. The effect of clusters on magnetic properties was also documented by other researchers [69, 70].

In the magnetic nanoparticles, there is the so-called blocking temperature or the energy barrier that can be obtained from ZFC and field-cooling (FC) magnetization curves. With increasing temperature, a curve peak should appear in the ZFC measurement. This peak temperature can be considered as the average T_B in the magnetic material. On the other hand, the increase of magnetic field should decrease the barrier energy, and results in a shift of the blocking temperature to lower temperatures. A typical of nanocrystalline Fe_3O_4 has shown superparamagnetic behavior (**Figure 3**). The superparamagnetism is related to the random fluctuation of the magnetization of a single domain when the thermal energy overcomes the anisotropy energy barrier. Below the T_B, the magnetization of each domain of nanoparticles is oriented parallel to a certain crystallographic direction or the easy axis with minimum energy. Consequently, the magnetization is blocked in the nanoparticles. Above T_B, the thermal energy can

http://dx.doi.org/10.5772/66293

overcome the anisotropy energy (barrier energy) and the magnetization starts fluctuating and the magnetic susceptibility follows modified Curie-law behavior at higher temperatures [71].

The effect of Mn^{2+} substitution on the magnetic properties of $Mn_xFe_{3-x}O_4$ nanoparticles has been intensively studied recently [54, 72]. It has been found that the lattice parameters and crystal volume of the $Mn_xFe_{3-x}O_4$ increase with the increase of Mn content. This is due to the fact that the ionic radius of Fe^{2+} is smaller than that of Mn^{2+} substituted in the spinel structure. Fe_3O_4 without any substitution has a cubic spinel structure, where the Fe^{2+} and Fe^{3+} ions occupy the tetrahedral (A) and octahedral (B) sites represented by $(Fe^{3+})_A(Fe^{3+}Fe^{2+})_BO^{2-}{}_4$. The Fe_3O_4 is one example of the cubic inverse spinels, in which there is a mixed valence of Fe ions on the octahedral sublattice. In the $Mn_xFe_{3-x}O_4$, the cationic distribution can be written as follows [54]:

$$\left(Mn_x^{2+}Fe_{1-x}^{3+}\right)_A\left[Fe_{1-x}^{2+}Fe_{1+x}^{3+}\right]_B \tag{6}$$

The Mn^{2+} ions occupy the A sites of the spinel structure. A further analysis of the SANS data of the $Mn_xFe_{3-x}O_4$ nanoparticles from $x = 0$ to 1 using the lognormal function has found that the particle size of the $Mn_xFe_{3-x}O_4$ depends on the Mn content. In this study, the increase of Mn content results in the smaller size of the nanoparticles. Moreover, the nanoparticles of $Mn_xFe_{3-x}O_4$ tend to become larger aggregates or clusters. The Mn content, particle size, and particle clustering are important factors influencing the magnetic properties of nanomaterials.

Taufiq et al. [55] have successfully synthesized Fe_3O_4 magnetic fluid with a chain-like spinel structure using coprecipitation method. These results show that the Fe_3O_4 ferrofluid has a primary particle size of about 7.6 nm and the size of fractal aggregates of about 45 nm constructing the chain-like structure. Even though there were chain aggregates, a homogeneous particle distribution with low polydispersity value of about 0.4 was found, which is lower than that in the former paper [55]. It is reported that both nanoparticles of Fe_3O_4 and $Mn_xFe_{3-x}O_4$ (x up to 1) exhibit superparamagnetic behavior and their saturation magnetization decreases with increasing Mn content [54, 72].

In the research of magnetic hydrogels, Fe_3O_4 ferrogels have been investigated by Sunaryono et al. [57]. It has been reported that the magneto-elastic properties of the ferrogels were strongly affected by the preparation technique, the ratio of the magnetic particle and the polymer, and magnetic particle content as well as the particle clustering and distribution. It has also been shown that the magneto-elasticity of the ferrogel tends to decrease with the increasing Fe_3O_4 content from 2.5 to 15% [56, 57]. Further analysis of the SAXS data using the two-lognormal distribution function showed that Fe_3O_4 in the hydrogel has primary particles of about 3 nm with an average particle distance of about 18 nm. Higher Fe_3O_4 concentration in the hydrogel leads to the increase of Fe_3O_4 cluster size. Due to the surface effect, it influences the magnetization value of the ferrogel. Consequently, the saturation magnetization drops with decreasing particle size and the cluster of Fe_3O_4 nanoparticles in the hydrogel. It has been confirmed that Fe_3O_4 ferrogel exhibits a superparamagnetic behavior at room temperature which is a crucial parameter for biomedical applications.

7.2. Improved mechanical properties of aluminum matrix composites with surfactant-coated $MgAl_2O_4$ nanofillers and $MgAl_2O_4$-coated SiC particulates

Figure 5 presents the XRD spectra (using Cu-Kα radiation, λ = 1.54 angstrom) of MgO and $MgAl_2O_4$ particles as results of coprecipitation process. The powders seem to be single phase as can be seen from the spectra, where no other additional diffraction peak is observed, except those associated with Miller indexes belonging to the MgO (periclase phase) and $MgAl_2O_4$ (spinel phase) as specified in **Figure 5**. Besides, the diffraction peaks are much broadened, featuring that the crystal is in nanometer size. If we take the full-width at half maximum (FWHM) of diffraction peaks, by using Scherrer formula [73] and taking the apparatus-broadening correction into account, we arrive at crystallite sizes of 17.5 ± 2.3 and 6.3 ± 0.7 nm for MgO and $MgAl_2O_4$ powders, respectively.

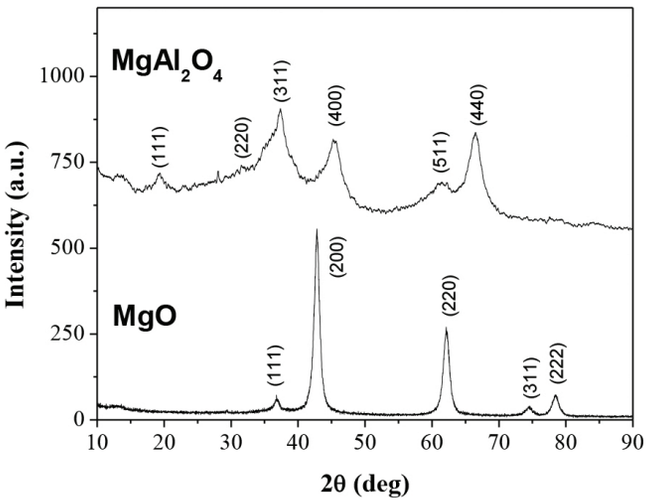

Figure 5. XRD spectra of MgO and $MgAl_2O_4$.

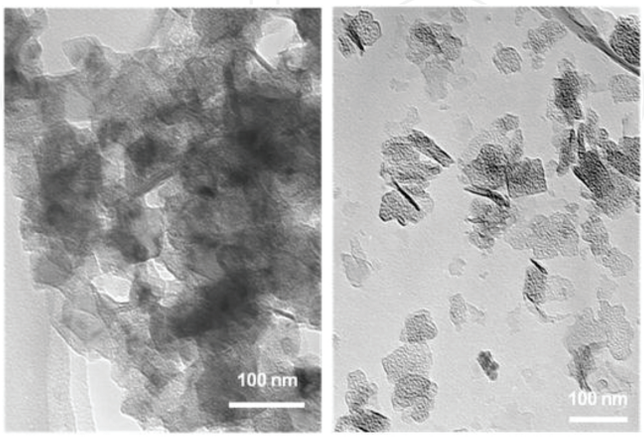

Figure 6. TEM images of (a) MgO and (b) $MgAl_2O_4$.

http://dx.doi.org/10.5772/66293

It is interesting to correlate the above crystallite size to the particle size of powders from TEM images depicted in **Figure 6**. The particle size for both powders, MgO in **Figure 6a** and $MgAl_2O_4$ in **Figure 6b**, is seen to be between 50 and less than 100 nm, confirming that the powders can be classified as nanoparticles. The shape of particles is observed to be varied from spherical, square, square with rounded edge, to semi-rod. Comparing the crystal and the particle sizes, one can consider that both MgO and $MgAl_2O_4$ powders contain secondary particles, where each particle is constituted by several crystals or grains.

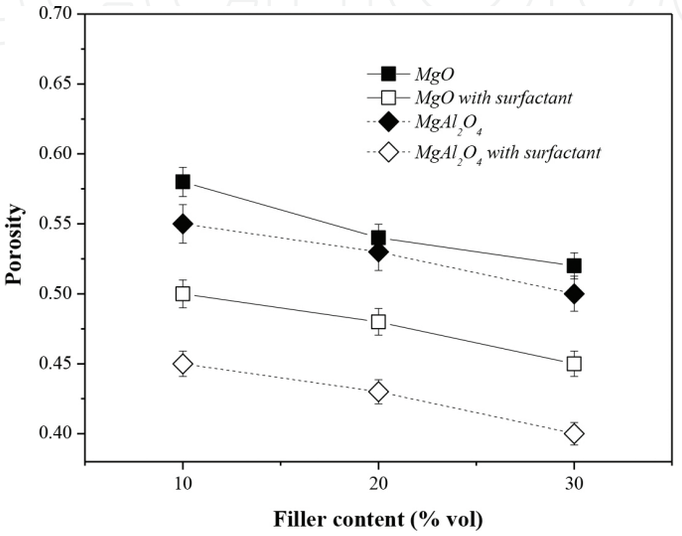

Figure 7. Porosity of sintered Al/MgO and Al/$MgAl_2O_4$ composites with fillers specified.

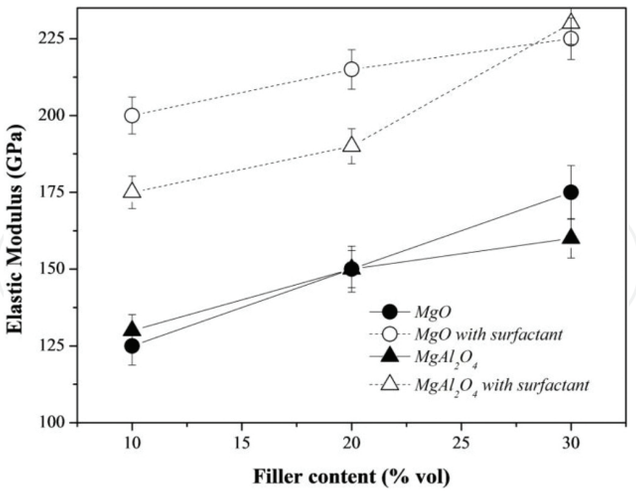

Figure 8. Elastic moduli of sintered Al/MgO and Al/$MgAl_2O_4$ composites with fillers specified.

To discuss further, the physical properties of composites, the density of pellets in the green state (after compaction) and after sintering significantly increases with increasing volume fraction of fillers and the use of surfactant (coated fillers by surfactant). The enhanced density

has led to the lowering porosity in the pellets. By applying the formula to define porosity [52]: $\rho = 1 - \rho_s/\rho_t$, where ρ_s and ρ_t stand for, respectively, sintered and theoretical densities, the porosity of samples is exhibited in **Figure 7**. The increase of pellet densification has directly affected the mechanical properties, as reflected by the results of compressive tests (yielding elastic modulus) and hardness (VHN) measurements (see **Figures 8** and **9**).

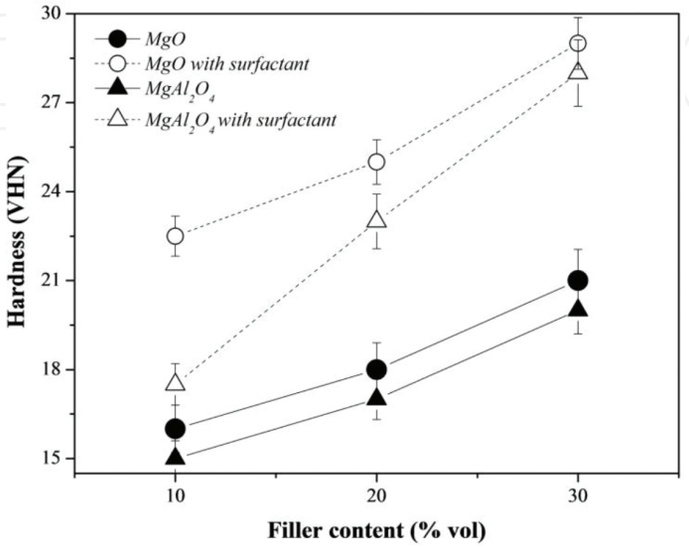

Figure 9. Micro-hardness of sintered Al/MgO and Al/$MgAl_2O_4$ composites with fillers specified.

It is worth noting that the role of surfactant is to enhance the physical and therefore mechanical properties of these Al/MgO and Al/$MgAl_2O_4$ nanocomposites. The TMAH as a mixing media of matrix and filler is an ionic molecule which will attach on the surface of nanoparticles. A metal-oxide nanoparticle is usually deficient of oxygen ion [74], hence its surface is positively charged. The negatively charged end of TMAH molecule is therefore attracted by metal-oxide surface, while the opposite end is dangled. It may further create the situation where one may consider that MgO or $MgAl_2O_4$ nanoparticle is "coated" by TMAH. This in turn avoids nanoparticles from aggregation to each other in the matrix. So, the filler is still in nanometer scale to maintain its larger surface area, especially compared to the agglomerated fillers having the same volume fraction in the composites fabricated without TMAH. The larger filler surface will lead to stronger interface bonding between matrix and filler.

The next attractive point to address is that the surfactant-coated MgO filler has led to considerably enhanced elastic modulus (~60%) and microhardness (~40%) of the Al-matrix nanocomposites (**Figures 8** and **9**). The periclase phase of MgO has simpler crystal structure than the spinel $MgAl_2O_4$ one [75, 76]. The former phase is transformed from $Mg(OH)_2$ at 500°C, whereas the latter one is already stable from 100°C as a result of coprecipitation process. Besides particles consolidation during the sintering at 500°C, the MgO filler will be possibly able to react further in a limited amount with Al matrix to form spinel phase on the matrix-filler interface, creating a strong bonding. Such kind of process, except consolidation, may not occur in the Al/$MgAl_2O_4$ composite, because of stable $MgAl_2O_4$.

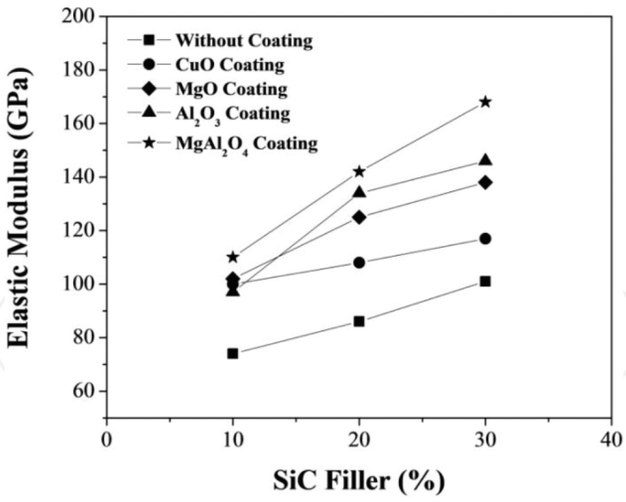

Figure 10. Elastic modulus of Al/SiC composites depending on filler content, using SiC coated by metal oxides as specified.

Going to further study on Al/SiC composites, it can be seen in **Figure 10** that a very clear distinction exists between SiC particles without coating and with coated metal oxides on the surface based on the modulus elasticity. The entire filler volume fraction (%vol) of SiC in Al-SiC composites using coatings has higher value than that without coating. The experimental results show that the modulus of elasticity of the composites using metal-oxide coating approaches the theoretical prediction [77], estimating a limit of lower and upper bounds. Based on the stress analysis, the composite having filler without metal oxide coating, for all low-volume fraction of reinforcement, the modulus value lies in the outside of the upper and lower bounds, which indicates weak interaction between matrix and filler. This is much different from composites with filler using metal oxides, where for the entire volume fraction of reinforcement, the elastic modulus lies inside the region of the upper and lower bounds, implying that the compactibility between matrix and filler, and reinforcements are therefore going well. One can see in **Figure 10** that coating with $MgAl_2O_4$ onto the SiC surface has produced the superior Al/SiC composites among the prepared samples, followed by Al_2O_3 and MgO. The three metal oxides coating materials mentioned seem to be compatible in facilitating and therefore enhancing interfacial bonding between Al matrix and SiC filler in the composites.

8. Conclusions

1. Fe_3O_4 and the $Mn_xFe_{3-x}O_4$ ($0 < x \leq 1$) nanoparticles have been successfully prepared by coprecipitation method utilizing a local natural source (viz. natural iron sand) as the main raw material.
2. The structures of Fe_3O_4 and $Mn_xFe_{3-x}O_4$ ($0 < x \leq 1$) nanoparticles, magnetic fluid, and magnetic hydrogel have intensively been studied by XRD, TEM, SANS, and SAXS data. These studies show that the magnetic materials have inverse spinel structure with a primary particle size of around 3–4 nm.

3. The magnetic properties have also been investigated by observing the hysteresis (M-H) behavior. It is found that Fe_3O_4 and $Mn_xFe_{3-x}O_4$ ($0 < x < 1$) nanoparticles exhibit superparamagnetic behavior at room temperature which depends on the particle size, doping content, and particle clustering.

4. The physical and mechanical properties of Al/MgO and Al/$MgAl_2O_4$ nanocomposites have been enhanced by the introduction of TMAH as surfactant during the mixing process of matrix and filler. The surfactant-coated MgO seems to be a more efficient filler compared to the surfactant-coated $MgAl_2O_4$ for the lower content (<30%). The experiment results show that the elastic modulus of the samples with volume fraction of fillers up to 30% was enhanced by more than 60% and 40%, respectively, for Al/MgO and Al/$MgAl_2O_4$. The use of other kind of surfactant needs to be explored to further enhance the mechanical properties.

5. A layer of the spinel $MgAl_2O_4$ micro-sized grown on the surface of SiC filler has induced the enhancement of mechanical properties of the Al/SiC composites.

Acknowledgements

This chapter is based on research partially supported by LPPM ITS, Ministry of Research and Technology, and Ministry of Education and Culture, Republic of Indonesia, 2006–2015.

Author details

Malik Anjelh Baqiya[1], Ahmad Taufiq[2], Sunaryono[2], Khuroti Ayun[1], Mochamad Zainuri[1], Suminar Pratapa[1], Triwikantoro[1] and Darminto[1*]

*Address all correspondence to: darminto@physics.its.ac.id

1 Advanced Materials Research Group, Department of Physics, Sepuluh Nopember Institute of Technology (ITS), Surabaya, Indonesia

2 Department of Physics, State University of Malang (UM), Malang, Indonesia

References

[1] D. Ghanbari, M. Salavati-Niasari, M. Ghasemi-Kooch, J. Ind. Eng. Chem. 20 (2014) 3970–3974.

[2] L.F. Cótica, V.F. Freitas, G.S. Dias, I.A. Santos, S.C. Vendrame, N.M. Khalil, R.M. Mainardes, M. Staruch, and M. Jain, J. Magn. Magn. Mater. 324 (2012) 559–563.

[3] F. Chen, S. Xie, X. Huang and X. Qiu, J. Hazard. Mater. 322 Part A (2017) 152–162.

[4] J. Sato, M. Kobayashi, H. Kato, T. Miyazaki, and M. Kakihana, J. Asian Ceram. Soc. 2 (2014) 258–262.

[5] T. Lu, J. Wang, J. Yin, A. Wang, X. Wang, and T. Zhang, Colloids Surf. A 436 (2013) 675–683.

[6] X. Zhang, D. Han, Z. Hua, and S. Yang, J. Alloys Compd. 684 (2016) 120–124.

[7] X. Cui, S. Belo, D. Krüger, Y. Yan, R.T.M. de Rosales, M. Jauregui-Osoro, H. Ye, S. Su, D. Mathe, N. Kovács, I. Horváth, M. Semjeni, K. Sunassee, K. Szigeti, M.A. Green, and P.J. Blower, Biomater. 35 (2014) 5840–5846.

[8] X. Zeng, B. Yang, X. Li, R. Li, and R. Yu, Mater. Des. 101 (2016) 35–43.

[9] C. Xingxing, Z. Xuebin, S. Hao, and F. Yi, Rare Met. Mater. Eng. 43 (2014) 2330–2334.

[10] C.-C. Lin and J.-M. Ho, Ceram. Int. 40 (2014) 10275–10282.

[11] I. Martínez-Mera, M.E. Espinosa-Pesqueira, R. Pérez-Hernández, and J. Arenas-Alatorre, Mater. Lett. 61 (2007) 4447–4451.

[12] A. Amirabadizadeh, H. Farsi, M. Dehghani, and H. Arabi, J. Supercond. Novel Magn. 25 (2012) 2763–2765.

[13] J.M. Niu and Z.G. Zheng, Adv. Mater. Res. 900 (2014) 172–176.

[14] H. Iida, K. Takayanagi, T. Nakanishi, and T. Osaka, J. Colloid Interface Sci. 314 (2007) 274–280.

[15] G. Gnanaprakash, S. Mahadevan, T. Jayakumar, P. Kalyanasundaram, J. Philip, and B. Raj, Mater. Chem. Phys. 103 (2007) 168–175.

[16] S. Lian, Z. Kang, E. Wang, M. Jiang, C. Hu, and L. Xu, Solid State Commun. 127 (2003) 605–608.

[17] D. Jin, G. Yongqian, C. Lanlan, Z. Guifu, L. Yue, and Q. Yitai, Nanotechnology 17 (2006) 4923.

[18] K. He, C.-Y. Xu, L. Zhen, and W.-Z. Shao, Mater. Lett. 61 (2007) 3159–3162.

[19] C. Scherer and A.M.F. Neto, Brazilian J. Phys. 35 (2005) 718–727.

[20] W. Yuan, C. Yin, P. Xiao, X. Wang, J. Sun, S. Huang, X. Chen, and Z. Cao, Microfluid. Nanofluid. 11 (2011) 781–785.

[21] C.L. Sansom, P. Jones, R.A. Dorey, C. Beck, A. Stanhope-Bosumpim, and J. Peterson, J. Magn. Magn. Mater. 335 (2013) 159–162.

[22] A. Labarta, J. Župan, and M.M. Renjo, 20th Int. Conf. Magn. ICM 2015, Physics Procedia, 75 (2015) 1458–1467.

[23] H. Ruican, L. Huagang, G. Wen, Z. Na, and H. Ruixiao, J. Magn. Magn. Mater. 416 (2016) 231–235.

[24] H. Ke, W. Huang, and X. Wang, Tribol. Int. 93, Part A (2016) 318–323.

[25] I. Sharifi, H. Shokrollahi, and S. Amiri, J. Magn. Magn. Mater. 324 (2012) 903–915.

[26] R.V. Ramanujan and L.L. Lao, Smart Mater. Struct. 15 (2006) 952.

[27] Y. Li, Z. Hu, and Y. Chen, J. Appl. Polym. Sci. 63 (1997) 1173–1178.

[28] M. Zrínyi, L. Barsi, and A. Büki, Polym. Gels and Networks, 5 (1997) 415–427.

[29] I. Ganesh, Int. Mater. Rev. 58 (2013) 63–112.

[30] I. Ganesh, B. Srinivas, R. Johnson, B.P. Saha, and Y.R. Mahajan, J. Eur. Ceram. Soc. 24 (2004) 201–207.

[31] H.B. Bafrooei and T. Ebadzadeh, Ceram. Int. 39 (2013) 8933–8940.

[32] P.Y. Lee, H. Suematsu, T. Yano, and K. Yatsui, J. Nanopart. Res. 8 (2006) 911–917.

[33] S. Tripathy and D. Bhattacharya, J. Asian Ceram. Soc. 1 (2013) 328–332.

[34] L.-Z. Pei, W.-Y. Yin, J.-F. Wang, J. Chen, C.-G. Fan, and Q.-F. Zhang, Mater. Res. 13 (2010) 339–343.

[35] S. Sanjabi and A. Obeydavi, J. Alloys Compd. 645 (2015) 535–540.

[36] M.F. Zawrah, H. Hamaad, and S. Meky, Ceram. Int. 33 (2007) 969–978.

[37] J. Rufner, D. Anderson, K. van Benthem, and R.H.R. Castro, J. Am. Ceram. Soc. 96 (2013) 2077–2085.

[38] H. Li, Y.Q. Liu, H. Liu, and Z.J. Yang, Mater. Res. Innovations, 19 (2015) S9-20-S29-23.

[39] A. Goldstein, J. Eur. Ceram. Soc. 32 (2012) 2869–2886.

[40] I. Ganesh, G. Jaganatha Reddy, G. Sundararajan, S.M. Olhero, P.M.C. Torres, and J.M.F. Ferreira, Ceram. Int. 36 (2010) 473–482.

[41] B. Ma, Y. Li, G. Liu, and D. Liang, Ceram. Int. 41 (2015) 3237–3244.

[42] S. Tripathy, D.S. Saini, and D. Bhattacharya, J. Asian Ceram. Soc. 4 (2016) 149–154.

[43] Z. Yu, N. Zhao, E. Liu, C. Shi, X. Du, and J. Wang, Composites Part A 43 (2012) 631–634.

[44] L. Xing, Y. Zhang, C. Shi, Y. Zhou, N. Zhao, E. Liu, and C. He, Mater. Sci. Eng., A 617 (2014) 235–242.

[45] Y. Zhou, Z. Yu, N. Zhao, C. Shi, E. Liu, X. Du, and C. He, Mater. Des. 46 (2013) 724–730.

[46] J.H. Boo, S.B. Lee, S.J. Ku, W. Koh, C. Kim, K.S. Yu, and Y. Kim, Appl. Surf. Sci. 169–170 (2001) 581–586.

[47] H. Jiang, Z. Cao, R. Yang, L. Yuan, H. Xiao, and J. Dong, Thin Solid Films, 539 (2013) 81–87.

[48] M.Y. Nassar, I.S. Ahmed, and I. Samir, Spectrochim. Acta, Part A 131 (2014) 329–334.

[49] P. Fu, W. Lu, W. Lei, K. Wu, Y. Xu, and J. Wu, Mater. Res. 16 (2013) 844–849.

[50] M.O. Bodunrin, K.K. Alaneme, and L.H. Chown, J. Mater. Res. Technol. 4 (2015) 434–445.

[51] E.T. Thostenson, C. Li, and T.-W. Chou, Compos. Sci. Technol. 65 (2005) 491–516.

[52] R.M. German, Liquid Phase Sintering, 1 ed., Springer US, New York, 1985.

[53] Sunaryono, A. Taufiq, Mashuri, S. Pratapa, M. Zainuri, Triwikantoro, and Darminto, Mater. Sci. Forum 827 (2015) 229-234.

[54] A. Taufiq, Sunaryono, E.G. Rachman Putra, A. Okazawa, I. Watanabe, N. Kojima, S. Pratapa, and Darminto, J. Supercond. Novel Magn. 28 (2015) 2855–2863.

[55] A. Taufiq, Sunaryono, E.G. Rachman Putra, S. Pratapa, and Darminto, Mater. Sci. Forum 827 (2015) 213–218.

[56] Sunaryono, A. Taufiq, Munaji, B. Indarto, Triwikantoro, M. Zainuri, and Darminto, AIP Conf. Proc. 1555 (2013) 53–56.

[57] Sunaryono, A. Taufiq, E.G.R. Putra, A. Okazawa, I. Watanabe, N. Kojima, S. Rugmai, S. Soontaranon, M. Zainuri, Triwikantoro, S. Pratapa, and Darminto, Nano, 11 (2016) 1650027.

[58] K.M. Wang, D.S. Lee, L. Horng, G. Chern, J. Magn. Magn. Mater. 282 (2004) 73–77.

[59] P.J. Reséndiz-Hernández, O.S. Rodríguez-Fernández, and L.A. García-Cerda, J. Magn. Magn. Mater. 320 (2008) e373–e376.

[60] E.G.R. Putra, Bharoto, E. Santoso, and A. Ikram, Nucl. Instrum. Methods Phys. Res., Sect. A 600 (2009) 198–202.

[61] F.L.O. Paula, R. Aquino, G.J. da Silva, J. Depeyrot, F.A. Tourinho, J.O. Fossum, and K.D. Knudsen, J. Appl. Crystallogr. 40 (2007) s269–s273.

[62] J. Teixeira, J. Appl. Crystallogr. 21 (1988) 781–785.

[63] M. Abboud, S. Youssef, J. Podlecki, R. Habchi, G. Germanos, and A. Foucaran, Mater. Sci. Semicond. Process. 39 (2015) 641–648.

[64] M. Gao, W. Li, J. Dong, Z. Zhang, and B. Yang, World J. Condens. Matter Phys. 1 (2011) 49–54.

[65] I. Volkov, S. Gudoshnikov, N. Usov, A. Volkov, M. Moskvina, A. Maresov, O. Snigirev, and S. Tanaka, J. Magn. Magn. Mater. 300 (2006) e294–e297.

[66] F.E. Osterloh, H. Hiramatsu, R.K. Dumas, and K. Liu, Langmuir, 21 (2005) 9709–9713.

[67] C. Daniela, C. Gabriel, and J.O.C. Charles, J. Phys. D: Appl. Phys. 40 (2007) 5801.

[68] P. Dutta, S. Pal, M.S. Seehra, N. Shah, and G.P. Huffman, J. Appl. Phys. 105 (2009) 07B501.

[69] M. Li, H. Gu, and C. Zhang, Nanoscale Res. Lett. 7 (2012) 1–11.

[70] S. Shen, S. Wang, R. Zheng, X. Zhu, X. Jiang, D. Fu, and W. Yang, Biomater. 39 (2015) 67–74.

[71] M. S. Seehra and A. Punnoose, Phys. Rev. B 64 (2001) 132410.

[72] J. Amighian, E. Karimzadeh, and M. Mozaffari, J. Magn. Magn. Mater. 332 (2013) 157–162.

[73] A.L. Patterson, Phys. Rev. 56 (1939) 978–982.

[74] Shipra, A. Gomathi, A. Sundaresan, and C.N.R. Rao, Solid State Commun. 142 (2007) 685–688.

[75] T.S. Duffy, C. Meade, Y. Fei, H.-K. Mao, and R.J. Hemley, Am. Mineral. 80 (1995) 222–230.

[76] L. Rooi Ping, A.-M. Azad, T. Wan Dung, Mater. Res. Bull. 36 (2001) 1417–1430.

[77] M. Zainuri, E.S. Siradj, D. Priadi, A. Zulfia, Darminto, MAKARA Sains, 12 (2008) 126–133.